Available online at www.sciencedirect.com
SCIENCE DIRECT®
Journal of Nuclear Materials 340 (2005) 163–170
journal of nuclear materials
www.elsevier.com/locate/jnucmat

Fabrication and microstructure characterization of inert matrix fuel based on yttria stabilized zirconia

Ch. Hellwig *, M. Pouchon, R. Restani, F. Ingold, G. Bart

Nuclear Energy and Safety Department, Paul Scherrer Institut, CH-5232 Villigen PSI, Switzerland

Received 24 September 2004; accepted 11 November 2004

Abstract

The deployment of a suitable, Pu-bearing inert matrix fuel (IMF) could offer an attractive option as a single-recycling LWR strategy aimed at reducing the currently growing plutonium stockpiles. A development programme focusing on yttria stabilized zirconia (YSZ)-based IMF is conducted at PSI. YSZ-based IMF has so far been irradiated in two test reactors. The fabrication routes as well as the characterization of the irradiated material by ceramography, electronprobe microanalysis, and X-ray diffraction are presented. IMF fabrication by attrition milling of the oxide constituents is possible, but high sintering temperatures are required to achieve homogeneity. X-ray diffraction is a suitable tool to monitor the homogeneity. Extra efforts are needed to increase the density.

PACS: 61.10.Nz; 61.16.Bg; 61.16.Ch; 81.05.Je

1. Introduction

Reprocessing is the key to an optimised utilisation of nuclear fuel. With the delayed development of fast reactors for closure of the fuel cycle, improvements to the industrial recycling of plutonium as uranium–plutonium oxide (MOX) in light water reactors (LWR) have recently been established in some countries whereas other countries are evaluating this option. Recycling of second and third generation plutonium as MOX in LWR after reaching a high burnup in each step seems economically less favourable. In this context, the deployment of a suitable, Pu-bearing inert matrix fuel (IMF) could offer an attractive option as a single-recycling LWR strategy aimed at reducing the currently growing plutonium stockpiles [1]. The suggestion of IMF was based on neutronic evaluations, aspects of safety and non-proliferation issues [2–5].

Material evaluations and investigations were performed to identify the most promising candidate material to be used as inert matrix [6–10]. A development programme focusing on material technology with the emphasis on fabrication and characterisation of the yttria stabilized zirconia (YSZ)-based IMF is conducted at PSI [11]. This type of material is stable under irradiation and not only neutronically but also chemically inert. This offers benefits with regard to the irradiation safety in an LWR, to final waste disposal and to proliferation concerns.

The YSZ-based IMF has so far been irradiated in the OECD Material Test Reactor in Halden [12,13] and in the High Flux Reactor in Petten [14]. Nevertheless, unexpectedly strong densification at beginning of irradiation determined by fuel stack elongation measurements in

* Corresponding author. Tel.: +41 56 310 2666; fax: +41 56 310 2203.
E-mail address: christian.hellwig@psi.ch (Ch. Hellwig).

0022-3115/$ - see front matter © 2004 Elsevier B.V. All rights reserved.
doi:10.1016/j.jnucmat.2004.11.004

Halden shows that the fabrication process must be improved.

An earlier publication focused mainly on the evolution of the microstructure of material produced by internal gelation [15]. The aim of this study was to compare the microstructures of IMF fabricated on two different routes, both after fabrication and after an additional re-sinter test, and to discuss possible improvements, especially for the material produced by the more industrially applicable attrition milling process.

2. Experimental

Two different routes have been utilised for the powder preparation to produce IMF pellets:

- dry mixing and milling of the oxide constituents in an advanced attrition mill [16] (IMF-Att) and
- co-precipitation in the form of microspheres by internal gelation with the desired composition of ZrO_2–$YO_{1.5}$–$ErO_{1.5}$–PuO_2, afterwards crushing the calcined microspheres in a mortar and milling of the shred in the attrition mill (IMF-Co).

2.1. Dry process

The oxide powders of the starting material (see Table 1) were first mixed mechanically by a rotator. The mixed powder was milled during 15 passes in the attrition mill.

2.2. Internal gelation

Micro-spheres were produced following the internal gelation process [17]. The concentrated nitrate solutions were prepared from the starting material referred in Table 2 and a plutonium nitrate solution. For the latter, the same PuO_2 powder as used for IMF-Att was dissolved in nitric acid with catalytic amounts of hydrofluoric acid. Am was separated before preparation of the so-called feed solution. Four batches of spheres with the composition of 73 at.%Zr–14 at.%Y–4 at.%Er–8 at.%Pu were produced. The applied gelation parameters are listed in Table 3. A vibrated nozzle was used for uniform droplets generation at a high throughput. The heat carrier was removed by trichloroethylene on belt filters and washing was performed with ammonia. The microspheres have been dried between 343 and 383 K in nitrogen atmosphere in a rotary dryer.

The four batches of dried micro-spheres were mixed together and calcined at 823 K in argon atmosphere. The loss in weight during calcination was 10.5 wt%. The calcined micro-spheres had a diameter of some 270 μm. They were crushed in an automatic mortar for 2 h and milled during 15 passes in the attrition mill.

Table 1
Oxide powders used for the fabrication of IMF-Att

	ZrO_2	Y_2O_3	Er_2O_3
Item no.	Z-2003	Y-2001	E-1015
Lot-no.	X17183-1	X13679T	X20379
Supplier	SOCCOCHIM AG/Lausanne		
Manufacturer		CERAC	
Purity (%)	99.95	99.99	99.9
Particle size (μm)	<3	≈1.25	≈2.30
Y_2O_3 content (wt%)	5.2	–	–
Hf content (wt%)	1.54	–	–
Concentration in mixture (wt%)	68.9	8.1	5.4
	PuO_2		
Values calc. to July 2000			
Pu content (wt%)	84.35		
Pu-fissile content (wt%)	62.85		
Am-241 content (wt%)	3.86		
Concentration in mixture (wt%)	17.6		

2.3. Pellet fabrication

Zinc stearate $Zn(C_{18}H_{35}O_2)_2$ as lubricant was added to the milled powder. The mixture was mechanically homogenized by a rotator for 1 h. The powders were then pre-compacted, granulated, compacted again to green pellets and sintered (see Table 4). The sinter conditions for IMF-Att were fixed according to tests reported in [11].

A re-sinter test was performed on three samples from each batch at 1973 K for 24 h in an $N_2 + 8\%H_2$-atmosphere.

Table 2
Starting materials used for IMF-Co micro-spheres fabrication (except Pu)

	Zirconyl nitrate	Yttrium nitrate	Erbium nitrate	HMTA	Urea
Formula	$ZrO(NO_3)_2 \cdot 2H_2O$	$Y(NO_3)_3 \cdot aq$	$Er(NO_3)_3 \cdot 5H_2O$	$(CH_2)_6N_4$	$CO(NH_2)_2$
Supplier	Interpolymer	FLUKA	ALDRICH	FLUKA	FLUKA
Purity (%)	–	>99	99.9	Purum	Purum p.a.
Hf content (wt%)	0.9	–	–	–	–

Table 3
Applied gelation parameters used for the IMF-Co microspheres fabrication

Metal concentration (mol kg^{-1})	0.6
Hexamethylenetetramine (HMTA) to metal (mol/mol)	1.20
Urea to metal (mol/mol)	0.03
Total nitrate to metal (mol/mol)	2.51
Gelation temperature (K)	374
Droplet size (μm)	≈900

Table 4
Pellet fabrication conditions for the two types of powders

	IMF-Att	IMF-Co
Pre-compaction pressure (MPa)	230	100
Compaction pressure (MPa)	480	500
Sinter temperature (K)	1723	1973
Sinter time (h)	6	6
Sinter atmosphere	CO_2 (i.e. oxidizing)	$N_2 + 8\%H_2$ (i.e. reducing)

2.4. Characterisation

The fabricated samples and samples additionally subjected to the re-sinter test were characterised with regard to geometrical density, microstructure, and homogeneity. The density was determined by the water immersion method. For the ceramography, the pellets were cut in axial direction, ground and polished. The IMF-Co pellets were etched chemically for the microstructure observation with an optical microscope, while it was not possible to etch the IMF-Att samples in the same way. Instead, thermal grooving was used to develop the grain boundaries in IMF-Att.

Tests at different temperatures were performed on YSZ in advance to determine the suitable grooving parameter under reducing atmosphere ($N_2 + 8\%H_2$). A good visibility of the grooves and the unmodified grain structure were the criteria for test conditions. Visible groove formation started on YSZ samples at 1573 K. The groove width – and thus the visibility – grew steadily with annealing temperature. The annealing temperature was restricted to 1873 K to avoid any change in microstructure. Some grain boundary movement could already be observed at relatively low temperatures, i.e. some small grains vanished. This effect was not significantly different for the higher temperatures. It was proposed that thin residuals of larger grains on the surface of the sample are removed due to the high diffusion rate at the ridges. Despite of these observations the grain size did not change significantly as those sharp-edged grains were small in number. The standard heating time was 1 h.

For thermal grooving of the fuel, the embedding resin was removed from the polished samples and the samples were first exposed to a temperature of 1723 K for 1 h. Both samples, the as-fabricated and the re-sintered one, showed very vague grain boundaries. Therefore, it was decided to repeat the procedure at 1873 K. No grain growth could be observed during thermal grooving of IMF. The grain sizes were determined using the linear intercept method and the results were multiplied with 1.56 to transform the two-dimensional results into three-dimensional grain size values [18].

Electronprobe microanalysis (EPMA) was performed on the ceramographic samples prior to etching or grooving. For X-ray phase analysis the samples were crushed to powder by a mortar and the measurement was performed on a diffractometer with $CuK\alpha_{1,2}$ radiation and nickel as internal standard for $\sin 2\theta$ calibration.

3. Results

The results of the density measurements are listed in Table 5. For the estimation of the relative density, the X-ray density (based on the measured lattice constants) was used as theoretical density (TD). IMF-Att was produced with a density typical for LWR fuel, whereas the fabrication of IMF-Co pellets was more difficult: several batches of IMF-Co were produced with densities between 85% and 92%TD (only the density of the batch involved in the re-sintering is shown in Table 5). The achieved densities depend on the applied sintering temperature; the higher the temperature, the higher the density. The re-sinter test shows a decrease in density for IMF-Att and a slight densification of 1.9%TD for IMF-Co.

Table 5
Results of the density measurements (determined by water immersion)

	IMF-Att	IMF-Co
As-fabricated		
Samples T232-1 (Att)/T226-1 (Co)	6.271	5.639
Samples T232-2 (Att)/T226-2 (Co)	6.274	5.735
Samples T232-3 (Att)/T226-3 (Co)	6.275	5.613
Mean geometrical density (g cm^{-3})	6.273	5.662
Relative density (% th.d.)	95.2	85.8
After re-sinter test		
Samples T232-1 (Att)/T226-1 (Co)	5.828	5.700
Samples T232-2 (Att)/T226-2 (Co)	5.819	5.856
Samples T232-3 (Att)/T226-3 (Co)	5.834	5.783
Mean geometrical density (g cm^{-3})	5.827	5.780
Relative density (% th.d.)	88.4	87.6

The as-fabricated and the re-sintered IMF-Att sample after the grooving procedure are shown in Figs. 1 and 2. The considerably large porosity is an artefact from sample preparation (chipped grains). Obviously, the as-fabricated sample shows much smaller grains in a very inhomogeneous structure. Some islands with tiny grains can be seen surrounded by larger grains. An evaluation of the grain size in these islands is difficult; however, a (three-dimensional) grain size of about 2.2 μm can be assigned. The major surface is dominated by larger grains of about 6.4 μm. The re-sintered sample has much larger grains, where an average grain size of 17 μm can be assigned, the grain structure is very homogeneous and the observed islands of tiny grains have vanished.

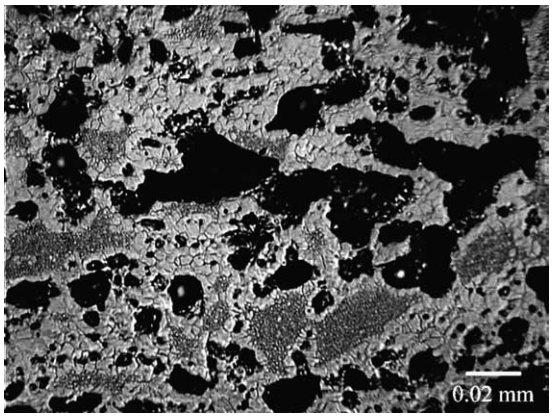

Fig. 1. Microstructure (developed by thermal grooving) of the as-fabricated IMF-Att pellet. The considerably large porosity is an artefact from sample preparation (chipped grains).

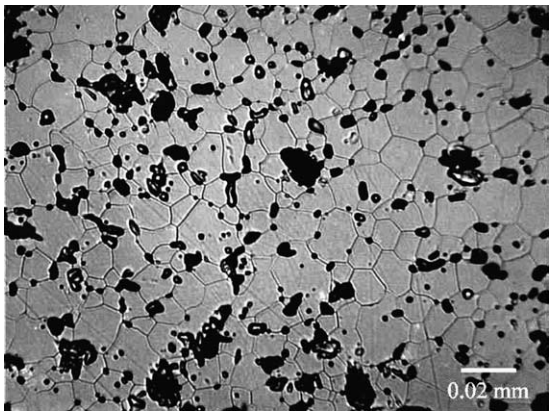

Fig. 2. Microstructure (developed by thermal grooving) of the re-sintered IMF-Att pellet. The considerably large porosity is an artefact from sample preparation (chipped grains).

In Fig. 3, the EPMA element distribution plot of Pu in the IMF-Att sample is depicted together with the SEM graph. Line scans from EPMA are plotted in Fig. 4. The as-fabricated material shows heterogeneities in the μm-range, with islands of nearly pure PuO_2. The IMF-Att is much more homogeneous after re-sintering as seen in Figs. 5 and 6.

Fig. 7 is a micrograph of a chemically etched section of IMF-Co. The grain size for IMF-Co was determined to 19 μm at the rim and to 28 μm in the centre of the pellet. IMF-Co has already in the as-fabricated condition a very homogeneous element distribution, see the typical local line scan in Fig. 8.

Fig. 9 gives an overview of the XRD patterns of the three investigated samples with Ni as internal standard. All XRD patterns show an fcc phase without any second phase. While the reflections of the as-fabricated IMF-Att are very broad, the reflections of the

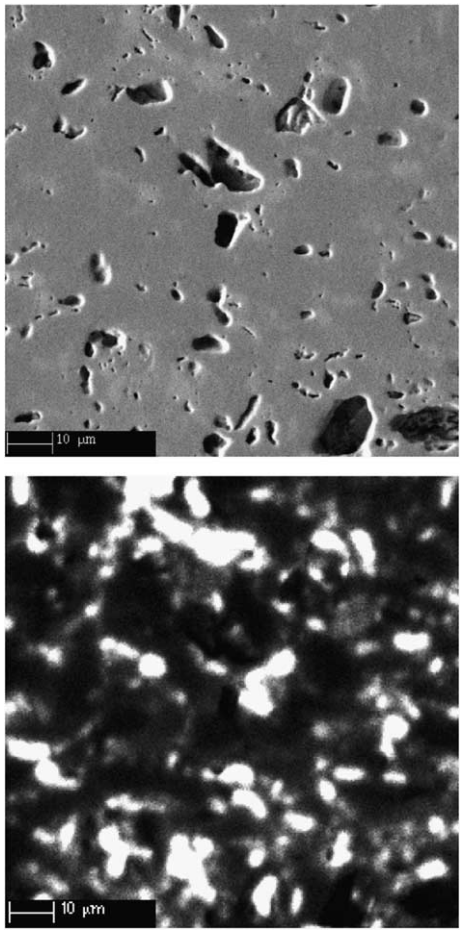

Fig. 3. EPMA pictures of as-fabricated IMF-Att: (top) SEM picture; (bottom) Pu-mapping. The bright islands in the bottom graph show nearly pure PuO_2 areas.

re-sintered IMF-Att and of IMF-Co are comparable in a relatively small full width at half maximum (FWHM).

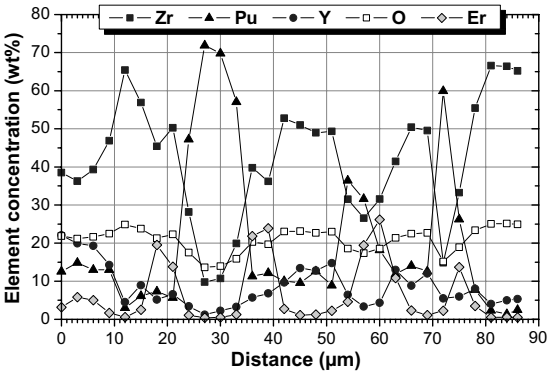

Fig. 4. EPMA line scans of the elements in as-fabricated IMF-Att (point analyses area $3 \times 3\ \mu m^2$).

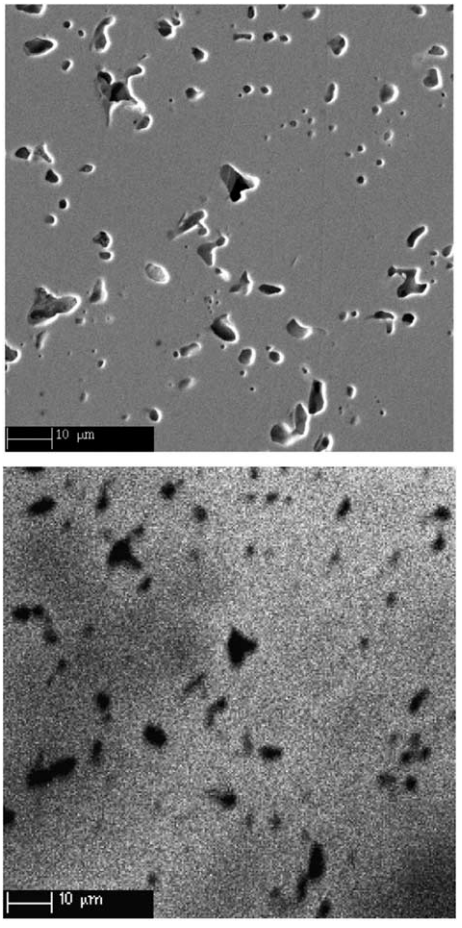

Fig. 5. EPMA pictures of re-sintered IMF-Att: (top) SEM picture; (bottom) Pu-mapping. The dark islands in the bottom graph are pores. Only slight Pu-variations are visible.

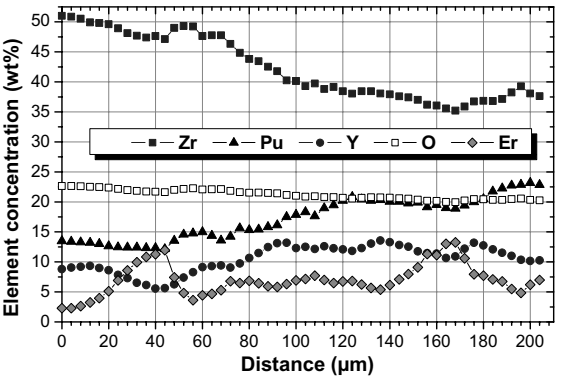

Fig. 6. EPMA line scans of the elements in re-sintered IMF-Att (point analyses area $3 \times 3\ \mu m^2$).

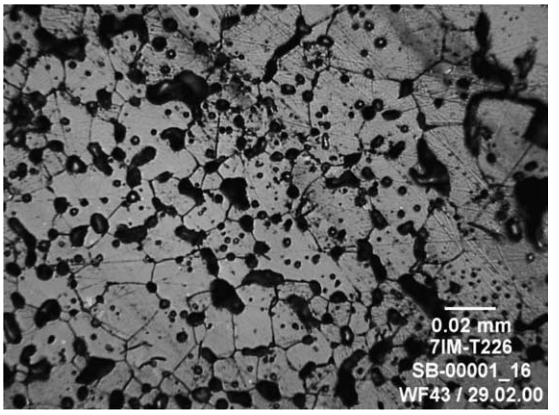

Fig. 7. Chemically etched microstructure of the center of an IMF-Co pellet.

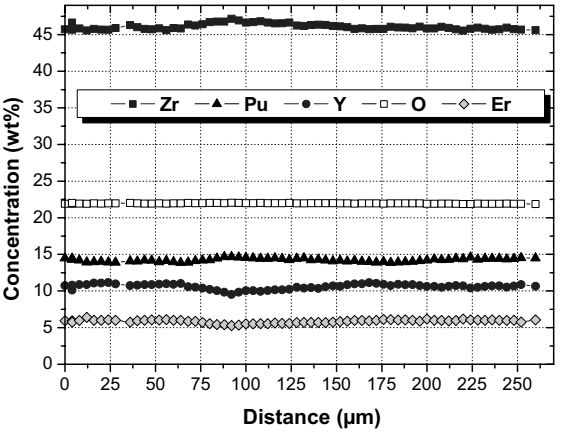

Fig. 8. EPMA line scans of the elements in as-fabricated IMF-Co (point analyses area $3 \times 3\ \mu m^2$).

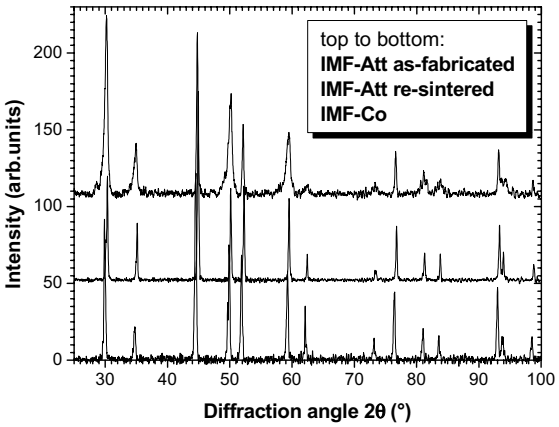

Fig. 9. Overview of the measured XRD patterns with nickel as internal standard (wavelength: 0.154178 nm).

Table 6
Evolution of the full width at half maximum (FWHM) for IMF-Att due to re-sintering (determined with $CuK\alpha_{1,2}$ radiation)

Reflection (hkl)	Bragg angle 2θ (°)	FWHM 2θ (°)	
		IMF-Att as-fabricated	IMF-Att re-sintered
111	30.32149	0.49287	0.27172
200	35.11379	0.58729	0.22006
220	50.1472	0.64484	0.22834
311	59.50625	0.74227	0.22306
222[a]	62.4198	2.12010	0.19391
400	73.39936	1.03343	0.33741
331	81.25564	1.24588	0.25642
420	83.78394	0.80566	0.19742

[a] Very weak reflection.

The lattice parameters are the same within the standard deviations:

IMF-Att as-fabricated: 0.517(1) nm,
IMF-Att resintered: 0.518(1) nm,
IMF-Co: 0.517(1) nm.

The evolution of the FMHW for most of the observed reflections is given in Table 6.

4. Discussion

While the density for the as-fabricated IMF-Att was found to be in a range common for LWR fuel, it was only possible to produce IMF-Co with significant lower density. The low sinter ability of IMF-Co is probably due to the fabrication process. The calcination step, i.e. the calcination temperature, could influence the sinter ability of the final powder. Also a more intense crushing and grinding of the calcined spheres could increase the sinter ability. Nevertheless, this fabrication route was not further investigated. IMF-Co is interesting for research as totally homogeneous material can be produced, but the process is too complicated for industrial powder production.

In contrast, IMF-Att exhibit good sinter ability but an unsatisfactory homogeneity on the microscopic level before re-sintering. EPMA and ceramography indicate clearly that IMF-Att in the as-fabricated condition is very heterogeneous in the μm range. The homogeneity could be much improved by the re-sintering, resp., by sintering at higher temperatures. For IMF-Co, the homogeneity observed by EPMA was nearly perfect, as expected.

The broad reflections observed in XRD reveal the presence of different compositions with the same crystal structure (fluorite structure, space group $Fm\bar{3}m$) but slightly different lattice constants. During the re-sinter test the material was homogenized and consequently the XRD pattern shows narrow reflections for the re-sintered material. If we assume (as a simplified extreme case for the following calculation) the as-fabricated material to consist of two separate phases, PuO_2 and YSZ, we can calculate the ratios of the expected intensities using the form factor of each component and then estimate the lattice constant that would derive from a superposition of both XRD patterns as listed in Table 7. Obviously, the material is more complex. There is a large variety of element distributions in solid solution, from areas very rich in Pu to areas very poor in Pu. Furthermore, more cations (Y^{3+}, Er^{3+}) with spatial variations are present in the fuel. Keeping this in mind and that peak shape fitting functions are involved in the determination of the lattice constant by XRD, the measured value of 0.517 nm can be well explained by superposition of reflections from different areas with different lattice parameters.

We can also see from Table 7 that the X-ray densities (mass of atoms per unit cell divided by the volume of unit cell) of the single phases are remarkably different mainly due to the mass differences. The X-ray density of an ideal solid solution yields to 6.505 g cm^{-3} (with an average mass of 544.5 g mol$_{\text{unit-cell}}^{-1}$ and a lattice constant of 0.518 nm). The volume average of the X-ray densities of the single phases yields to 6.616 g cm^{-3}. Thus, the geometrical density of IMF-Att in the as-fabricated condition would drop to 93.6%TD instead of 95.2%TD, i.e. the porosity would be 6.4% instead of 4.8%.

However, this is not the main reason for the large decrease of density (from 6.273 g cm^{-3} to 5.827 g cm^{-3}) during the re-sinter test. The relatively small deviation of the measured densities of the three IMF-Att pellets subjected to the re-sinter test (see Table 5) indicates that

Table 7
Characteristics of the unit cells of YSZ, PuO_2 and an ideal mixture of 9 mol% PuO_2 in YSZ

	$(F_{PuO_2}/F_{YSZ})^2$[a]	Lattice parameter[b] (nm)	Mass per mol unit-cells (g)	X-ray density (g cm^{-3})
YSZ	≈5.88	0.5125	491	6.057
PuO_2		0.5397	1085	11.461
Superposition of two phases		≈0.5225	–	6.616[c]
Ideal mixture		0.518	544.5	6.505

[a] The X-ray intensities depend on $|F|^2$ (where F is the form factor). The given values have been calculated as an average of the ratios for the reflections listed in Table 3.

[b] See Ref. [19] for YSZ; the PuO_2-data and the ideal mixture (re-sintered IMF-Att) were measured in our laboratory, the value for the two-phase superposition was calculated using the concentration and the X-ray intensities.

[c] Average calculated by taking into account the concentration and the volume ratio.

a 'random' process like crack formation is not involved. Taking into account the strongly reducing atmosphere during the re-sinter test, the formation of the pyrochlore-type phase $Pu_2Zr_2O_7$ must also be considered. It has been demonstrated that this phase can be formed under Ar + 8%H_2 atmosphere at 1973 K [20]. Nevertheless, the XRD results show unambiguously a single-phase fluorite structure without any extra reflections, for both, re-sintered IMF-Att and as-fabricated IMF-Co. The lattice constant of the pyrochlore-type phase $Pu_2Zr_2O_7$ is given with 1.0614 nm in the above mentioned reference. This represents a duplication of the lattice constant of the fluorite structure due to the formation of a superlattice. Comparing this lattice constant with the average of PuO_2 and YSZ lattice constants leaves only small potential for swelling due to phase transformation (about 2.8% volume increase). Therefore a large and clearly detectable fraction of the material would have to be transformed to achieve the measured volume increase. In YSZ the cubic phase is stabilized by Y^{3+} and Er^{3+} as they replace Zr^{4+} and thus introduce oxygen vacancies (possible cation-size effects [21] shall be ignored for this discussion). Pu is expected to be present as Pu^{4+} but might contribute to the oxygen vacancies if it is reduced to Pu^{3+}. Nevertheless, the composition investigated in this work contains some 77 at.% of tetravalent cations (Zr^{4+}) which obviously prevent the formation of the pyrochlore-type phase $Pu_2Zr_2O_7$ where 50% of the cations being trivalent (Pu^{3+}).

The formation of extra porosity during sintering or re-sintering is a well-known process for ceramics when the original powder contains carbon or chlorine impurities. While the impurities in the commercial powders were accurately controlled, the specification of the used Pu lists only vague values of <150 ppm for carbon and chlorine. Impurities in the Pu-powder might also explain the reported differences in achieved densities between inactive tests (with Ce instead of Pu) and test with Pu-containing material [5]. It is interesting to note that MOX fabricated on the same route as IMF-Att and using the same Pu-powder was also sintered under oxidative atmosphere at 1723 K, followed by a reducing step under N_2 + 8%H_2 at 1473 K. The achieved density was some 95%TD but after the re-sinter test at 1973 K, a density decrease of 3.5%TD was observed. A gas-forming reaction of the impurities that occurs at high temperatures is therefore a possible explanation for the density decrease during re-sintering.

During irradiation the fuel centre temperatures are calculated to be more than 1800 K. Under neutron flux and helium a significant densification at beginning of irradiation was observed, i.e. roughly 100%TD was achieved [7]. This proofs that the sinter activity of the irradiation-activated material was high enough and the pores were small enough to allow a complete annihilation of the porosity. It cannot be decided (and is of no practical consequence) if the annihilation overrules the formation of additional porosity or if under these in-pile conditions the formation of additional porosity is suppressed.

5. Conclusions and outlook

With IMF-Att and IMF-Co two very different powders have been used for the fabrication of YSZ-based IMF pellets. The homogeneity of IMF-Co is nearly perfect but the process is complicated and it seems to be difficult to achieve high densities.

In principle, IMF fabrication is possible by attrition milling of the oxide constituents. Although the homogenization in the μm-range is difficult, higher sintering temperatures can be applied to achieve a homogeneous material; the atmosphere seems to be of minor importance. A satisfying density of completely sintered material could not yet be achieved, further research with plutonia of higher purity is required. X-ray diffraction delivers valuable information about the homogeneity of the products and the progress in the sintering process.

The results of this investigation will also be used to characterize the alterations of grain size and homogeneity under irradiation as soon as first PIE results from Halden are available.

Acknowledgments

We gratefully acknowledge the fuel production work of P. Heimgartner. The fuel fabrication became possible by the collaboration with KAERI (D.S. Sohn, Y.-W. Lee, H.S. Kim). The authors would also like to thank the Swiss utilities (swissnuclear) for the financial support of the actinide and fuel research work at PSI.

References

[1] R. Chawla, R.J.M. Konings, Prog. Nucl. Energy 38 (2001) 455.
[2] H. Akie, T. Muromura, H. Takano, S. Matsuura, Nucl. Technol. 107 (1994) 182.
[3] C. Degueldre, U. Kasemeyer, F. Botta, G. Ledergerber, Mater. Res. Soc. Symp. Proc. 412 (1995) 15.
[4] U. Kasemeyer, J.M. Paratte, P. Grimm, R. Chawla, Nucl. Technol. 122 (1998) 52.
[5] A. Stanculescu, U. Kasemeyer, J.M. Paratte, R. Chawla, J. Nucl. Mater. 274 (1999) 146.
[6] R.J.M. Konings, K. Bakker, J.G. Boshoven, H. Hein, M.E. Huntelaar, R.R. van der Laan, J. Nucl. Mater. 274 (1999) 84.
[7] H. Kleykamp, J. Nucl. Mater. 275 (1999) 1.
[8] H. Serizawa, K. Nakajima, Y. Arai, T. Yamashita, K. Kuramoto, H. Kinoshita, S. Yamanaka, M. Uno, K. Kurosaki, Prog. Nucl. Energy 38 (2001) 237.
[9] L. Thomé, A. Gentils, F. Garrido, J. Jagielski, Prog. Nucl. Energy 38 (2001) 277.
[10] V.V. Rondinella, T. Wiss, Hj. Matzke, R. Mele, F. Bocci, P.G. Lucuta, Prog. Nucl. Energy 38 (2001) 291.
[11] G. Ledergerber, C. Degueldre, P. Heimgartner, M.A. Pouchon, U. Kasemeyer, Prog. Nucl. Energy 38 (2001) 301.
[12] Ch. Hellwig, U. Kasemeyer, G. Ledergerber, B.-H. Lee, Y.-W. Lee, R. Chawla, Ann. Nucl. Energy 30 (2003) 287.
[13] C. Hellwig, U. Kasemeyer, J. Nucl. Mater. 319 (2003) 87.
[14] R.P.C. Schram, R.R. van der Laan, F.C. Klaassen, K. Bakker, T. Yamashita, F. Ingold, J. Nucl. Mater. 319 (2003) 118.
[15] M. Burghartz, G. Ledergerber, F. Ingold, P. Heimgartner, C. Degueldre, Prog. Nucl. Energy 38 (2001) 247.
[16] Y.W. Lee, H.S. Kim, S.H. Kim, C.Y. Joung, S.H. Na, G. Ledergerber, P. Heimgartner, M.A. Pouchon, M. Burghartz, J. Nucl. Mater. 274 (1999) 7.
[17] G. Ledergerber, F. Ingold, R.W. Stratton, H.P. Alder, C. Prunier, D. Warin, M. Bauer, Nucl. Technol. 114 (1996) 194.
[18] M. Hirai, J.H. Davies, R. Williamson, J. Nucl. Mater. 226 (1995) 238.
[19] R.P. Ingel, D. Lewis III, J. Am. Ceram. Soc. 69 (1986) 325.
[20] S. Yamazaki, T. Yamashita, T. Matsui, T. Nagasaki, J. Nucl. Mater. 294 (2001) 183.
[21] S.D. Conradson, C.A. Degueldre, F.J. Espinosa-Faller, S.R. Foltyn, K.E. Sickafus, J.A. Valdez, P.M. Villella, Prog. Nucl. Energy 38 (2001) 221.